Cell Reports
Physical Science

CellPress
OPEN ACCESS

Article

Thermomechanical activation achieving orthogonal working/healing conditions of nanostructured tri-block copolymer thermosets

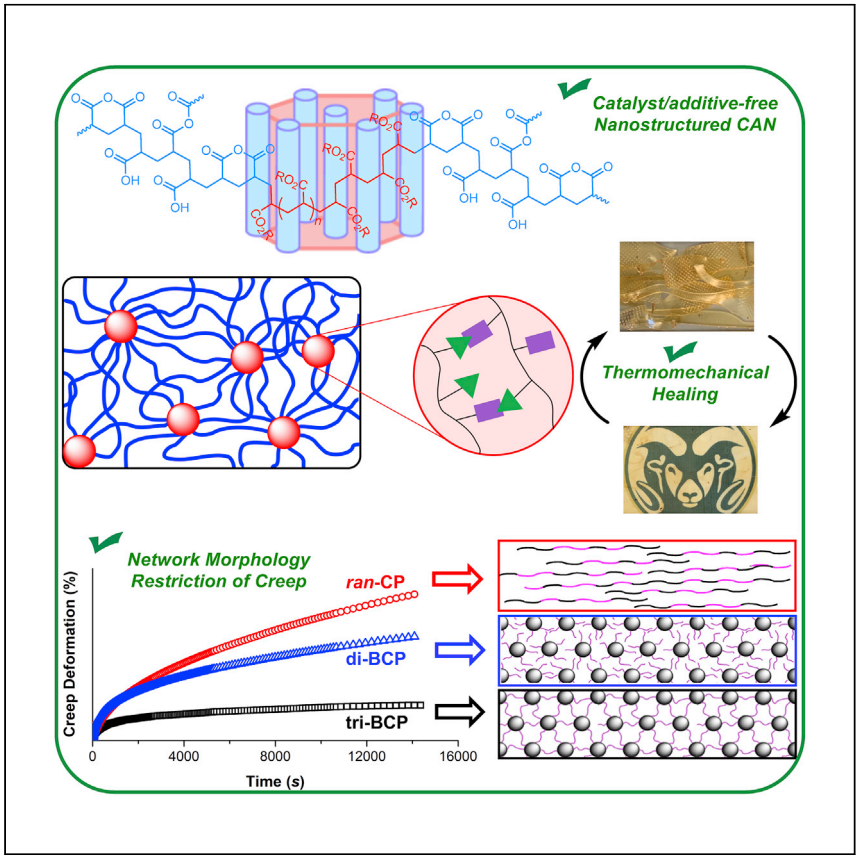

Clarke et al. show crosslinked tri-block copolymers with nanostructured networks, constructed by a catalyst/additive-free self-crosslinking and self-assembly process. Compared with analogous random and di-block copolymers, these crosslinked tri-block copolymers show not only superior mechanical performance but also much greater creep resistance when operated on a morphology-regulated and thermomechanical activation mechanism.

Ryan W. Clarke, Michael L. McGraw, Brian S. Newell, Eugene Y.-X. Chen

eugene.chen@colostate.edu

Highlights

Tri-BCP assembly into additive-free, inter-linked hexagonally packed cylinder networks

Healable crosslinked networks via thermomechanical-induced inter-domain bond exchange

Working conditions restrict creep, establishing orthogonal working/healing behavior

Clarke et al., Cell Reports Physical Science 2, 100483
July 21, 2021
https://doi.org/10.1016/j.xcrp.2021.100483

Please cite this article in press as: Clarke et al., Thermomechanical activation achieving orthogonal working/healing conditions of nanostructured tri-block copolymer thermosets, Cell Reports Physical Science (2021), https://doi.org/10.1016/j.xcrp.2021.100483

Cell Reports
Physical Science

Article

Thermomechanical activation achieving orthogonal working/healing conditions of nanostructured tri-block copolymer thermosets

Ryan W. Clarke,[1] Michael L. McGraw,[1] Brian S. Newell,[2] and Eugene Y.-X. Chen[1,3,*]

SUMMARY

Conventional thermosets, despite their technological significance in today's materials economy, present a modern sustainability challenge because of their lack of end-of-life options for recyclability or reprocessability. Emerging covalent adaptable networks (CANs) offer sustainable alternatives to permanently crosslinked materials, but ideal orthogonal working/reprocessing conditions are hardly achievable by the current thermochemical activation mechanism. Here we report a CAN system of additive/catalyst-free, fully reprocessable, crosslinked, tri-block copolymer (tri-BCP) thermoplastic elastomer networks based on acid-anhydride bond exchange operated on a thermomechanical activation mechanism. The unique functionality of the tri-BCP architecture enables self-assembly into interlinked, hexagonally packed cylinder nanostructures that preclude any productive inter-cylinder bond exchange (and, thus, creep) without cooperative thermal and mechanical (heating and compression) processing conditions.

INTRODUCTION

The ever-growing materials economy has recently begun to reevaluate its prioritization of several competing ends. Although, in the past, factors such as cost, utility, and scalability alone influenced which materials were mass produced, today's modern perspectives on global sustainability have incentivized consideration of factors such as renewability, recyclability, reprocessability, and environmental impact.[1–12] Several strategies have been put forth to address these new challenges, including, notably, design of intrinsically recyclable polymers,[13–15] repurposing or upcycling of post-consumer commodity plastics,[16–20] and enabling reprocessability of crosslinked thermosets by utilizing innovative concepts of vitrimers,[21–28] covalent adaptable networks (CANs),[29–47] and non-covalent self-healing networks.[48] Common requirements for achieving a CAN or vitrimer system include privileged functional groups, multiple synthetic steps, or added catalysts and crosslinkers. Such dynamically crosslinked thermosets can enter their flow state upon activation of covalent bond exchange reactions photo- or thermochemically (with light or heat and/or a catalyst).[30,31,35,42,45,49] An example of polyhydroxyurethane vitrimers via transcarbamoylation activated by mechanical stress has also been reported.[50]

Applications that demand crosslinked materials require resistance to creep (deformation), heat (melting), and solvents (dissolution). Ideal CANs or vitrimers should be capable of resisting dissolution and creep at working temperature and stress while only entering the flow state during reprocessing conditions. Achieving

[1]Department of Chemistry, Colorado State University, Fort Collins, CO 80523-1872, USA

[2]Molecular and Materials Analysis Center, Colorado State University, Fort Collins, CO 80523-1872, USA

[3]Lead contact

*Correspondence: eugene.chen@colostate.edu

https://doi.org/10.1016/j.xcrp.2021.100483

Please cite this article in press as: Clarke et al., Thermomechanical activation achieving orthogonal working/healing conditions of nanostructured tri-block copolymer thermosets, Cell Reports Physical Science (2021), https://doi.org/10.1016/j.xcrp.2021.100483

such ideal orthogonal behavior would make CANs sustainable alternatives to conventional thermosets. Creep at working temperature and stress is an important challenge for CANs. Recent efforts to improve creep resistance were directed toward morphology-tunable block copolymers (BCPs).[51–55] For example, several advantages have been reported in a di-BCP system where the poly(*n*-butyl methacrylate) (P^{n}BMA) block exists in domains separated from the vitrimeric domain furnished by poly(2-acetoacetoxyethyl methacrylate) blocks with an added xylylene diamine cross-linker via dynamic transamination.[21] Most notably, the lamellar phase-separated di-BCPs exhibited superior resistance to creep compared with random copolymer analogs, which was explained by noting that phase separation localizes crosslinked domains, resulting in higher crosslinking density, which restricts "network strand diffusion."

The phase-separated domain morphology is an ideal platform to test our hypothesis that bond exchange events that occur within one isolated domain are not productive in reconfiguring material shape. In other words, exchange-driven permanent deformation might only be achieved by inter-domain exchange or mixing. To test this hypothesis, we need to investigate effects of higher block architectures; in particular, an ABA tri-BCP system with crosslinking and exchange points contained within the A-blocks inter-linked by the soft B-blocks. Here, each crosslinking A-domain should be connected to other A-domains, generating one continuous macro-network. In contrast, the AB di-BCP system theoretically forms a discontinuous network where each hard domain is disconnected from the next. Thus, it is foreseeable that permanent macro-phase deformation can be a source of creep.[56] Recent tri-BCP work utilized a post-functionalized tri-BCP with dynamic bond exchange in localized poly(4-pyridine) terminal domains with the added alkyl dibromide crosslinker by trans-*N*-alkylation, but creep and reprocessability were not addressed.[28] Combining the two synergistic concepts of ABA networking and inter-domain exchange, we endeavored to identify an intriguing scenario where neither thermal energy nor mechanical force alone is enough to induce creep, and only the collaborative effort of both can achieve productive permanent deformation because thermal energy is needed to induce dynamic bond exchange, whereas mechanical force is needed to induce inter-domain contact.

To this end, we developed a high-performance, self-assembling, and reprocessable tri-BCP network system (Figure 1A) by utilizing ubiquitous carboxylic acids and anhydrides of simple acrylic monomers where poly(acrylic acid) (PAA) units are crosslinked through a well-known acid/acid condensation of water (forming an anhydride).[57,58] Recognizing the fact that this crosslinking reaction, which occurs at temperatures of more than 150°C, does not go to completion, we reasoned that the residual carboxylic acid (Figure 1B) could serve as an exchange agent by attacking the anhydride crosslink in poly(acrylic anhydride) (PAAn) to eliminate a carboxylate equivalent, thus cleaving the crosslink (Figures 1C and 1D). If supported, then this would mean that nearly any polymer or copolymer containing acrylic acid units could foreseeably be converted into a CAN without the need for any additional reagents, catalysts, or crosslinkers. Because there are already several known methodologies that can produce copolymers of PAA, including thermal decomposition of poly(*tert*-butyl acrylate) (P^{t}BA) to PAA,[59–63] several variations of dynamic materials can be immediately targeted with this concept. For this study, we employed our recently disclosed compound sequence control (CSC) Lewis pair polymerization (LPP) methodology[64] to access high-molecular-weight (MW), all-acrylic ABA tri-BCPs (generation 1 [G1]; Figure 1A) to study synergistic self-assembly and discrete networking effects, compared with other CAN architectures, on creep resistance to

Please cite this article in press as: Clarke et al., Thermomechanical activation achieving orthogonal working/healing conditions of nanostructured tri-block copolymer thermosets, Cell Reports Physical Science (2021), https://doi.org/10.1016/j.xcrp.2021.100483

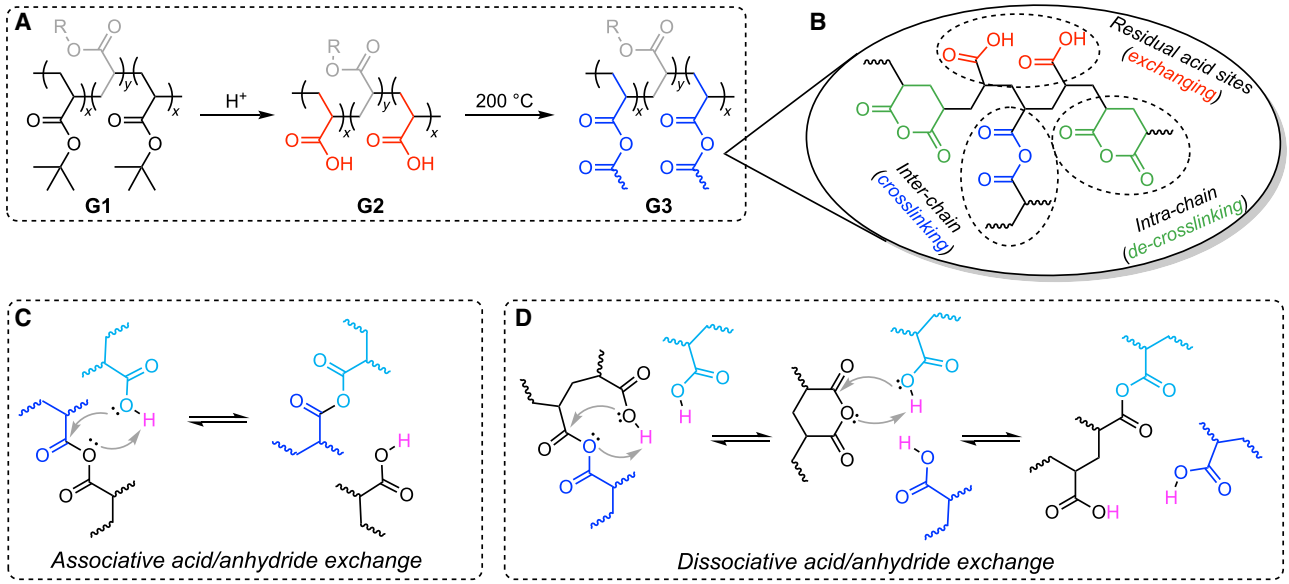

Figure 1. All-acrylic ABA tri-BCP CANs via acid-anhydride exchange

(A) Selective transformation of P^{t}BA-containing BCPs (G1) into PAA (G2) and PAAn (G3) BCPs.

(B) Possible structures of PAAn network polymer.

(C) Postulated inter-chain associative exchange mechanism between residual acid and crosslinked anhydride units.

(D) Postulated intra-chain dissociative exchange mechanism between residual acid and crosslinked anhydride units.

develop a superior collaborative thermomechanical exchange mechanism for orthogonal working/reprocessing conditions in CAN-type materials.

RESULTS

Small-molecule acid-anhydride associative exchange models

To provide evidence to support the postulated dynamic exchange between a carboxylic acid and an anhydride, we set out to investigate this possible exchange reaction using small-molecule models.[29–39] Using ^{19}F NMR, we monitored 2-h bulk exchange reactions between 4,4,4-trifluorobutyric acid (TFBA) and stearic anhydride (SAn) at 25°C, 100°C, and 150°C under inert conditions. The evolution of one fluorinated species (triplet) at 25°C into three, accounting for all exchange products and TFBA (Figure 2), beginning at 100°C supports our postulated exchange mechanism (Figures 1C and 1D). The exchange products were further characterized by quadrupole time-of-flight mass spectrometry (Q-TOF-MS), revealing masses for all expected exchange structures (Figures 2, S1, and S2).

Conceivably, the dynamic acid-anhydride exchange can occur as intra-chain between two neighboring acids to form a cyclic anhydride (decrosslinking) or inter-chain to form a linear anhydride (crosslinking) (Figures 1C and 1D).[58] We also considered parallel self-exchange between local anhydrides in the absence of acid groups, which has been hypothesized previously.[65] Using a similar approach, we found successful exchange by Q-TOF-MS between decanoic anhydride and SAn at 100°C (Figure S3); for this reason, we do not rule out the possibility of competing anhydride-anhydride self-exchange.

Synthesis of all-acrylic tri-BCPs and G1-to-G2-to-G3 evolution

Our designed hard-soft-hard ABA tri-BCP precursor to thermoplastic elastomer (TPE) CANs has a general structural formula of PAA-*b*-PAE-*b*-PAA, where the crosslinkable PAA end-blocks can be readily derived from the selective acid-catalyzed

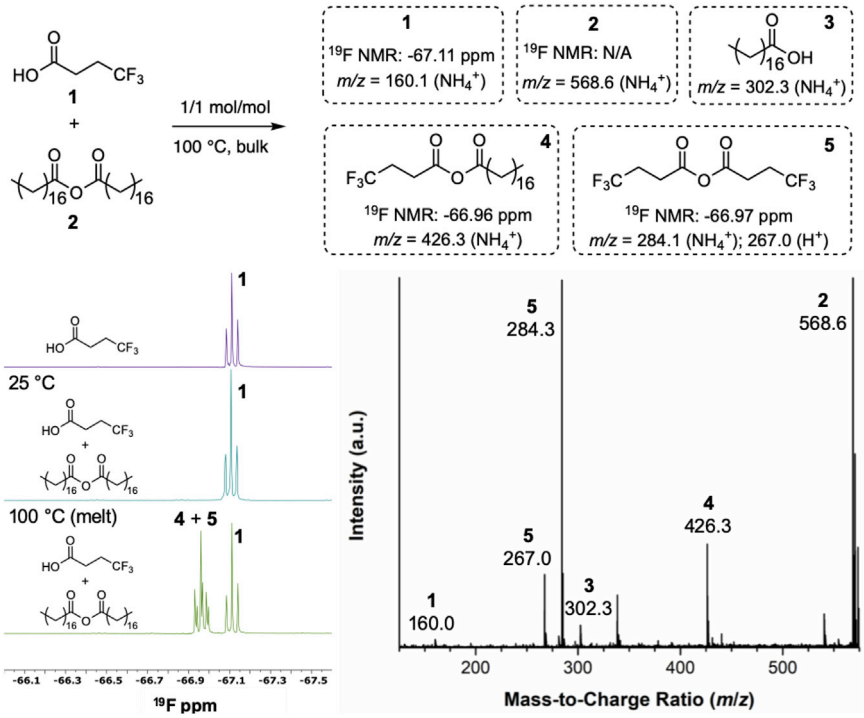

Figure 2. Evidence of acid-anhydride exchange at high temperature

Depicted are results of small-molecule proxy experiments for the proposed paralleling acid-anhydride associative and dissociative exchange mechanisms utilizing ^{19}F NMR and Q-TOF-MS (NH_4^+).

de-*tert*-butylation[66] of P^{t}BA blocks, and the middle (soft) block can be a flexible, low glass-transition temperature (T_g) poly(acrylic ester) (PAE), such as poly(methyl acrylate) (PMA) or poly(*n*-butyl acrylate) (P^{n}BA). We envisioned that such tri-BCPs could be readily synthesized using our recently established CSC-LPP methodology.[64]

We first utilized LPP to synthesize high-MW homopolymers for tensile model studies (Figure 3A), including PMA (M_n = 1.13 × 10^5 g mol^{-1}, $Đ$ = 1.08), P^{n}BA (M_n = 1.03 × 10^5 g mol^{-1}, $Đ$ = 1.07), and P^{t}BA (M_n = 1.88 × 10^5 g mol^{-1}, $Đ$ = 1.11) (Table S1). Next, the model study for transformation of G1 P^{t}BA blocks to (G2) PAA blocks and, last, to G3 crosslinked PAAn blocks (i.e., G1-to-G3 tri-BCP transformation) was performed. Specifically, G1 P^{t}BA was transformed near-quantitatively into G2 PAA via acid (trifluoroacetic acid [TFA])-catalyzed elimination of isobutene from the ^{t}Bu-ester (Figure 1A).[59,61] Heat treatment of PAA at 150°C–200°C results in condensation of two carboxylic acid units, observable by DSC, to yield an acrylic anhydride in the form of the intra-chain rigid backbone and inter-chain crosslinker, G3 PAAn (Figures 1A, 1B, and S23).

Using the CSC-LPP method (Figure 3B), we synthesized high-MW (M_n > 10^5 g mol^{-1}) G1 tri-BCPs at three different hard-soft-hard volume ratios (1:2:1, 1:3:1, and 1:8:1): P^{t}BA$_{500}$-*b*-P^{n}BA$_{1,000}$-*b*-P^{t}BA$_{500}$ (M_n = 2.71 × 10^5 g mol^{-1}, $Đ$ = 1.03), P^{t}BA$_{150}$-*b*-P^{n}BA$_{450}$-*b*-P^{t}BA$_{150}$ (M_n = 1.12 × 10^5 g mol^{-1}, $Đ$ = 1.07), and P^{t}BA$_{100}$-*b*-PMA$_{800}$-*b*-P^{t}BA$_{100}$ (M_n = 1.45 × 10^5 g mol^{-1}, $Đ$ = 1.08) (subscripts note the target degree of polymerization in synthesis; Figures S4–S6). Full synthesis, characterization, and mechanical testing of parent G1 copolymers is discussed in greater detail in Figures S10–S12, S16–S19, S24–S28, and S32–S33 and Table S2).

Cell Reports
Physical Science
Article

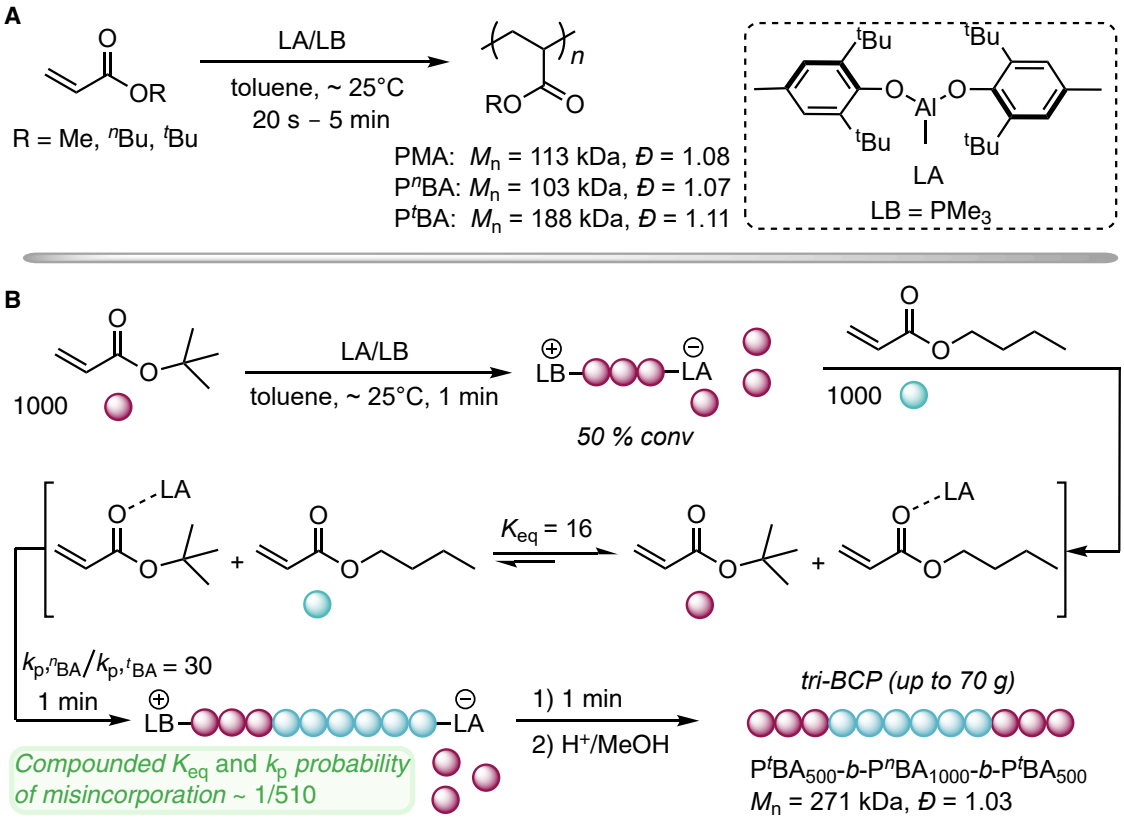

Figure 3. Outlined polymer synthesis by LPP

(A) Synthesis of homopolymer controls.

(B) Synthesis of tri-BCPs (represented by ^{t}BA and ^{n}BA).

Following the same G1-to-G3 evolution protocol established for homopolymer P^{t}BA, the above P^{t}BA-containing parent BCPs (G1) were selectively transformed into PAA (G2) and PAAn (G3) BCPs. The G1-to-G2 transformation was nearly quantitative (98.7%– 99.6%; Figures S34–S36; Table S3), affording G2 PAA$_{100}$-*b*-PMA$_{800}$-*b*-PAA$_{100}$, PAA$_{500}$-*b*-P^{n}BA$_{1,000}$-*b*-PAA$_{500}$, and PAA$_{150}$-*b*-P^{n}BA$_{450}$-*b*-PAA$_{150}$ tri-BCPs. The G2 BCPs were simultaneously molded into films and crosslinked into G3 network BCPs by compression molding at 200°C under 5,000 psi. As anticipated, all G3 network BCPs are insoluble in common solvents (only swelling), resistant to acids (e.g., 12 M HCl), and soluble/degradable through hydrolysis in 1 M aqueous NaOH, supporting crosslinking by inter-chain anhydrides (Figure S40). Thermal stability of the reprocessable G3 materials was also supported by measuring mass lost during a 1-h isothermal event at 200°C, which revealed a negligible decline to 99.0%– 99.6% initial mass (Figures S43–S48). The G3 network BCPs, PAAn-*b*-PAE-*b*-PAAn, were thermally crosslinked—without any reagent, linker, or catalyst—selectively at the PAA domains that were predesignated during synthesis of the G1 BCPs.

Mechanical properties of G1/G2/G3 tri-BCPs

The mechanical properties of G1/G2/G3 tri-BCPs with two different middle soft blocks (PMA and P^{n}BA) are summarized in Figure 4A and Tables S9–S26, with representative tensile stress-strain curves depicted in Figures 4B and 4C. Additional tensile experiments, such as cyclic strain deformation highlighting G2 TPE characteristic elasticity,[67,68] shape memory, and evolution of tensile profiles with tri-BCP generations G1–G3 are described in Figures S38, S39, and S59 and Tables S4 and S5. Strips

A

BCP (G#)	Strength (MPa)	Modulus (MPa)	Elongation (%)	Toughness ($MJ \cdot m^{-3}$)
PAA_{100}-*b*-PMA_{800}-*b*-PAA_{100} (G2)	2.2 ± 0.3	0.5 ± 0.07	978 ± 55	7.4 ± 0.6
$PAAn_{100}$-*b*-PMA_{800}-*b*- $PAAn_{100}$ (G3)	42 ± 1.0	2870 ± 366	123 ± 16	40 ± 6.6
PAA_{500}-*b*-$P^{n}BA_{1000}$-*b*-PAA_{500} (G2)	11 ± 0.7	4.2 ± 0.2	342 ± 16	19 ± 1.6
$PAAn_{500}$-*b*-$P^{n}BA_{1000}$-*b*-$PAAn_{500}$ (G3)	22 ± 1.0	22 ± 13	269 ± 19	33 ± 2.0
PAA_{150}-*b*-$P^{n}BA_{450}$-*b*-PAA_{150} (G2)	3.1 ± 0.2	2.7 ± 0.2	156 ±7.0	2.8 ± 0.3
$PAAn_{150}$-*b*-$P^{n}BA_{450}$-*b*-$PAAn_{150}$ (G3)	19 ± 2.9	351 ± 35	208 ± 24	37 ± 2.4

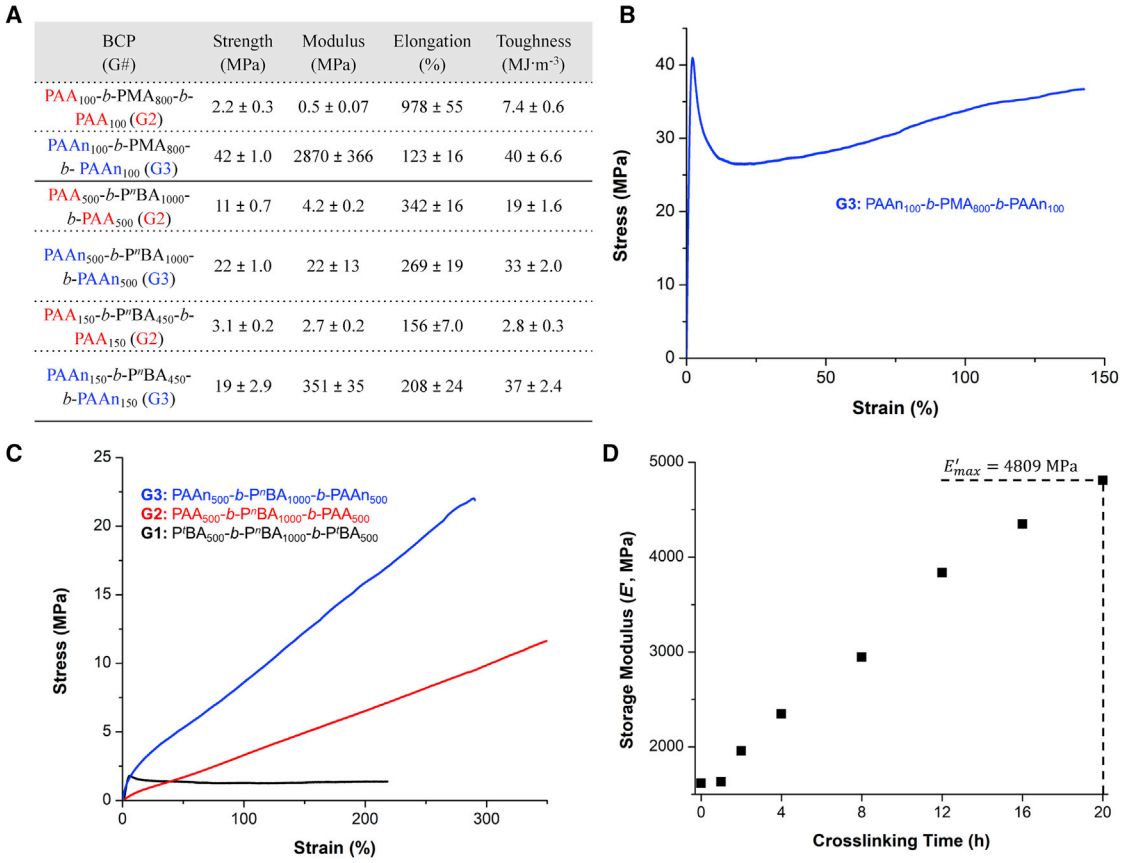

Figure 4. Tensile properties of G1–G3 tri-BCPs

(A) Tensile profiles of selected G1/G2/G3 tri-BCPs. Values are based on 3–5 averaged dog bone specimens (5 mm/min, ~23°C; see also Tables S9–S26).

(B) Representative tensile stress-strain curve (5 mm/min, ~23°C) of G3 network tri-BCP $PAAn_{100}$-*b*-PMA_{80}-*b*-$PAAn_{100}$.

(C) Representative tensile stress-strain curves (5 mm/min, ~23°C) of tri-BCPs: $P^{t}BA_{500}$-*b*-$P^{n}BA_{1,000}$-*b*-$P^{t}BA_{500}$ (G1, black), PAA_{500}-*b*-$P^{n}BA_{1000}$-*b*-PAA_{500} (G2, red), and $PAAn_{500}$-*b*-$P^{n}BA_{1,000}$-*b*-$PAAn_{500}$ (G3, blue).

(D) Relationship between maximum storage modulus (E') over crosslinking time for G3 $PAAn_{100}$-*b*-PMA_{800}-*b*-$PAAn_{100}$ by DMA (−50°C to 150°C, 5°C/min, 0.3% strain, 1 Hz).

of G3 $PAAn_{100}$-*b*-PMA_{800}-*b*-$PAAn_{100}$ films crosslinked for 0 (G2), 1, 2, 4, 8, 12, 16, 20, and 24 h were subjected to dynamic mechanical analysis (DMA) temperature-ramp frequency sweeps (−50°C to 150°C, 5°C/min, 0.3% strain, 1 Hz) to track the evolution of mechanical and thermal behavior with crosslinking time (Figure 4D). As expected, the uncrosslinked G2 specimen yielded the lowest modulus while failing below 100°C (Figure S49). Crosslinked G3 specimens exhibited increasing moduli over time to a high modulus maximum of 4.81 GPa (Figures 4D and S49; Table S6), indicating drastically increased film hardness. Samples above 20 h of crosslinking time reached a plateau in modulus performance (Figure S50). Each crosslinking time-point sample was also analyzed by Fourier transform infrared (FTIR) spectroscopy, revealing no observable structural changes or indications of decomposition (Figure S42). The T_g values of the PMA block at G2 and each crosslinking time point were determined similarly through DMA by locating the temperature of the tan δ_{max}, revealing an immediate jump in T_g by more than 14°C upon going from G2 to G3 (Figure S49; Table S6). Additional frequency sweeps to 200°C revealed a stable rubbery plateau ($\Delta E' \approx$ constant) indicating thermomechanical stability at high operating temperatures for thermoset applicability in each of the G3 tri-BCP CANs (Figures S51 and S52).

Please cite this article in press as: Clarke et al., Thermomechanical activation achieving orthogonal working/healing conditions of nanostructured tri-block copolymer thermosets, Cell Reports Physical Science (2021), https://doi.org/10.1016/j.xcrp.2021.100483

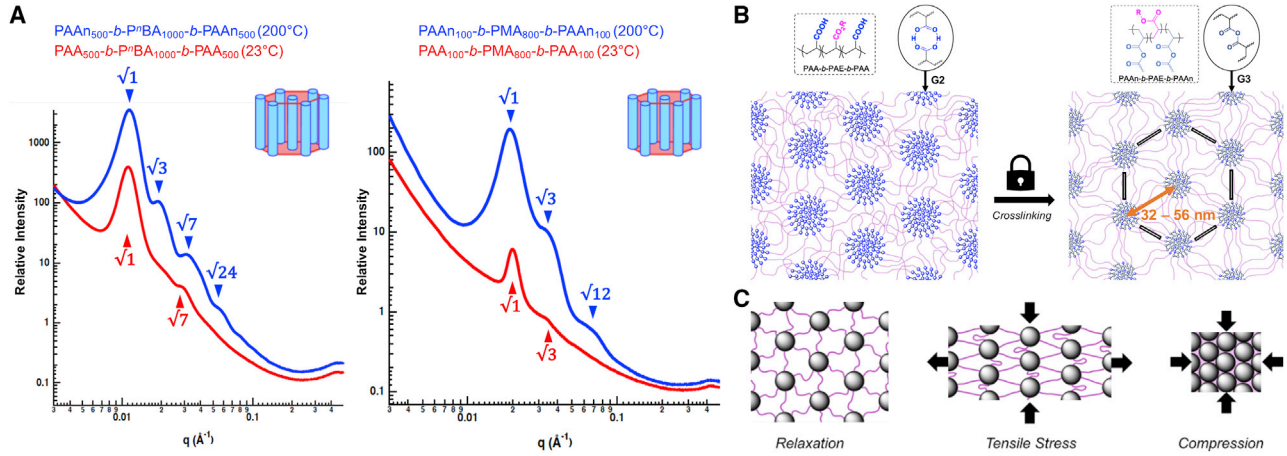

Figure 5. Self-organizing, crosslinking, and reinforcing

(A) SAXS profiles of tri-BCP films in G2 PAA (red, measured at 23°C) and G3 crosslinked PAAn (blue, measured at 200°C) HPCs.

(B) Illustrative nanostructural crosslinking of self-assembled G2 H-bonded PAA sites (left) into covalently linked PAAn G3 network BCP domains (right).

(C) Postulated chain physics of the HPC crosslinked G3 network tri-BCP at relaxation, tensile stress, and compression conditions.

When subjected to tensile tests, the G3 tri-BCPs drastically outperformed the G2 homologs in tensile strength and modulus (Figures 4A–4C; Table S7). In particular, $PAAn_{100}$-*b*-PMA_{800}-*b*-$PAAn_{100}$ exhibited an impressive plastic character with a high Young's modulus E of ~2.9 ± 0.37 GPa, ultimate tensile strength σ_B of ~42 ± 1.0 MPa, and elongation at break ε_B of ~123% ± 16% (Figure 4B), reflecting ~5,700×, ~20×, and ~5.4× enhancement in modulus, strength, and toughness, respectively, compared with its G2 homolog (Figure 4A). A similar trend, albeit to a lesser degree, was also observed for the BCPs with P^{n}BA as the soft block upon advancing to the G3 BCP network (Figures 4A and 4C).

Self-assembly of G2/G3 BCPs and crosslinked G3 TPE networks

Recognizing the advantageous functionality induced by self-assembly into phase-separated nanostructures in various reported BCP systems,[69–71] we envisioned that the presence of the PAA hard blocks in tri-BCPs could effectively utilize H-bonding to self-assemble into discrete acid domains. Flash-heating during compression molding of these G2 BCPs with phase-separated PAA domains could then permanently link into covalently bound tri-BCP PAAn-PAE-PAAn networks. Accordingly, films of PAA_{100}-*b*-PMA_{800}-*b*-PAA_{100} and PAA_{500}-*b*-P^n$BA_{1,000}$-*b*-PAA_{500} were analyzed by small-angle X-ray scattering (SAXS) to reveal the phase behavior of these BCPs at ambient (23°C) and elevated (200°C) temperatures (Figure 5A).

Scattering for each BCP sample was collected at 23°C and again at 200°C after 30 min of bulk thermal annealing. Both BCPs exhibited scattering patterns consistent with hexagonally packed cylinder (HPC) self-assembled nanostructures with domain spacings (d_{100}) in a range of 32–56 nm (Figure 5B; calculations are shown in the Supplemental information). This observation infers that, at 200°C, both BCPs retain and improve the HPC packing, where the hard domains (PAA and PAAn) comprise the cylinders. Noteworthy here is that we did not observe order-disorder transition temperatures at 200°C, indicating retention and stability of these complex architectures at reprocessing temperatures. Less intense scattering peaks prior to crosslinking can likely be attributed to the non-covalent, looser HPC packing. Figure 5C depicts the self-assembled PMA-containing G3 CAN with inter-cylinder links, connecting each cylinder to its neighbors. Thus, when the HPC structure is

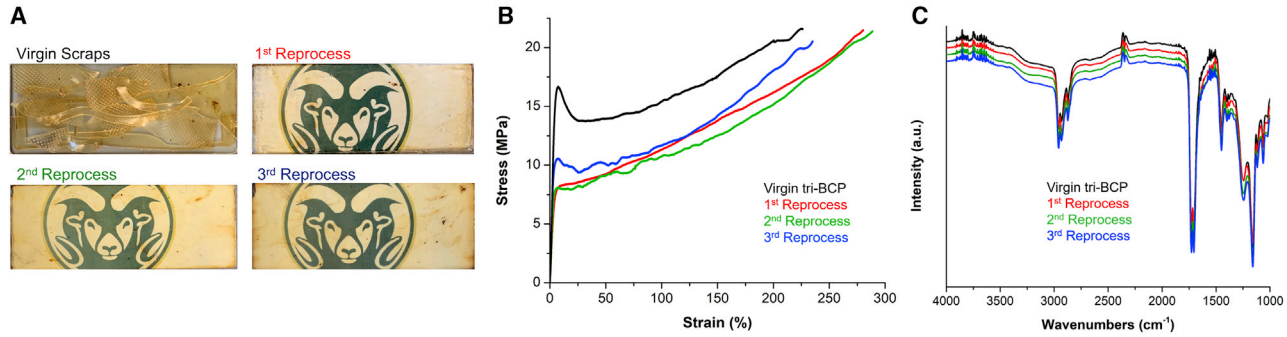

Figure 6. Reprocessability of acid-anhydride CANs

(A) Photographed films of (3×) thermomechanically reprocessed G3 CAN tensile scraps.

(B) Stress-strain curves (5 mm/min, ~23°C) of virgin and reprocessed $PAAn_{150}$-*b*-P^nBA_{450}-*b*-$PAAn_{150}$ films.

(C) FTIR spectral overlays for virgin and reprocessed $PAAn_{150}$-*b*-P^nBA_{450}-*b*-$PAAn_{150}$ films.

relaxed, there can be a small degree of mobility for each cylinder because of the flexibility of the soft PMA block. However, when tensile stress is applied, the PMA linkers tighten and immobilize the entire structure. This reasoning can also account for the sizable yield point and high modulus observed for this G3 material (Figure 4B).

Thermomechanical reprocessability of G3 CANs

Conventional thermosets seldom permit any reprocessability as a result of the complex, dense network of random covalent crosslinks unless they become dynamically exchangeable under processing conditions; this is the case with CANs. A consistent compression molding pressure of 5,000 psi was chosen for reprocessing G3 BCP scraps, whereas a temperature of 200°C was selected in compliance with observed mild endothermic delineation onsets in 3× heating-cycle DSC traces at this temperature (Figure S60).

Accordingly, we added the scraps from the $PAAn_{150}$-*b*-P^nBA_{450}-*b*-$PAAn_{150}$ tensile tests to the compression mold and subjected them to reprocessing conditions. After reprocessing, what were once deformed scraps had become a homogeneous film (Figure 6A). Reprocessed G3 CAN materials exhibited nearly complete, if not superior (within error), mechanical recovery (Table S8). For example, the tensile strength and elongation were maintained in the range of 19–22 MPa and 208%–285%, respectively, over the four consecutive reprocessing cycles (Figure 6B; Table S8). We also observed that reprocessed G3 CANs exhibited a lower yield strength than the virgin sample, which could be attributed to two possible chemical events occurring during reprocessing conditions. One is oxidation of anhydride units, which would decrease the overall crosslinking density, and the second is the shift in the ratio of intra-molecular (decrosslinking) and inter-molecular (crosslinking) anhydrides to the higher-energy cyclic analog, which would similarly decrease the crosslinking density. In either case, FTIR spectra revealed that the structural constitution of the TPE CANs, including hydroxyl-region absorption bands, are retained in each life cycle (Figure 6C).

Because the G3 reconfigurable networks cannot rearrange because of the locked interworking of the nanostructure (Figure 5B), our remaining hypothesis to explain reprocessability is the inter-cylinder acid-anhydride exchange, which allows crosslink mixing between cylinders (Figure 5C). If transformation from G2 to G3 results in a critical maximum number of anhydride bonds, then there should be residual acrylic acid units present, which should trigger the bond exchange at high temperatures (Figures 1C

and 1D). Residual acid units were characterized by FTIR analysis of the PAAn homopolymer (Figure S41). Exchange within one cylinder would likely be non-productive. Therefore, thermal compression of the HPC-structured G3 network is needed to push exchange-active domains into proximity of colliding with each other (Figure 5C) so that acid-anhydride exchange can occur between chains/cylinders.

Rheological properties of G3 BCP CANs

To further probe the recovery nature of the current BCP-based CANs, rheology was employed to observe the material behavior under high-temperature bulk shearing conditions. We reasoned that, because the G3 inter-linked network architecture requires unique, cooperative thermal-compression conditions to achieve productive exchange, the tri-BCPs would not be suitable for investigating prolonged creep or stress relaxation and, thus, the acid-anhydride exchange mechanism activation energy. As a result, we utilized non-sequencing LPP to synthesize a random copolymer (RCP), P^nBA_{520}-*ran*-P^tBA_{350} (3:2 for comparison to 1:3:1 tri-BCP, M_n = 112 kDa, $Đ$ = 1.02; Figures S7, S13, S20, S29, and S37), which would be unable to assemble into discrete, inter-crosslinked nanostructures and, thus, experience macro-scale deformation by dynamic bond exchange without thermal compression events. The RCP, upon advancing to its G3 CAN following the same methods, exhibited excellent reprocessability and full mechanical recovery within 30 min of reprocessing, as opposed to the typical 24 h of thermal compression (Figure S61; Table S8). In the absence of the discretely inter-linked exchange domains, the delocalized G3 dynamic crosslinks experience the typical thermochemical CAN tradeoff: facile reprocessing but significantly amplified creep. We explore and establish the thermomechanically exclusive inter-domain exchange mechanism through creep, frequency sweep, and stress-relaxation experiments, discussed below.

Bulk creep/resistance experiments were performed on the acid-anhydride CANs to investigate material integrity over prolonged stress. An initial investigation of the evolution of creep displacement (5 kPa, 100°C for G1 and G2 BCPs, 150°C for G3 BCP), modeled by the PMA-containing tri-BCP set, highlights a significant increase in creep resistance upon advancing G1 to G2 (by 22%) and G2 to G3 (by 29%) as a direct result of the respective hydrogen-bonding and crosslinking-network self-reinforcement (Figure 7A). Following an initial strain increase accounted for by the material's inherent flexibility, G3 BCP $PAAn_{100}$-*b*-PMA_{800}-*b*-$PAAn_{100}$ showed negligible shear creep (<0.3%) at 150°C, whereas the uncrosslinked G1 and G2 homologs exhibited pronounced creep even at a lower temperature of 100°C. Prolonged creep experiments were performed on each G3 CAN over a 4-h period at an elevated temperature of 200°C (5 kPa), revealing high-performance creep resistance by all G3 tri-BCPs (Figure S55). Specifically, all tri-BCPs exhibited a negligible creep rate between 2.5–4.1 × 10^{-5}% shear strain per second and low creep values (<2% shear strain over 4 h), excluding the initial spike in strain via intrinsic material flexibility (Figures 7A–7C and 5C). As expected, and in support of our proposed morphology-regulated productive exchange mechanism, the G3 RCP exhibited noticeably higher creep deformation (11.8% versus 1.1%) and deformation rates (5.9 × 10^{-4} versus 3.4 × 10^{-5}% shear strain per second) over the 4-h stress event compared with its tri-BCP compositional analog (Figure 7B). To provide further support for the specific ABA triblock architecture functionality, the authors prepared a compositionally equivalent (3:2, P^nBA_{900}-*b*-P^tBA_{600}, M_n = 2.99 × 10^5 g mol^{-1}, $Đ$ = 1.08; Figures S8, S14, S21, and S30) AB di-BCP by CSC-LPP that, conceivably, should be unable to form an inter-domain crosslinked network when crosslinked and, thus, experience deformation in the absence of compression. In agreement, the G3 P^nBA_{900}-*b*-$PAAn_{600}$ di-BCP exhibited pronounced creep (5.5%) over the 4-h

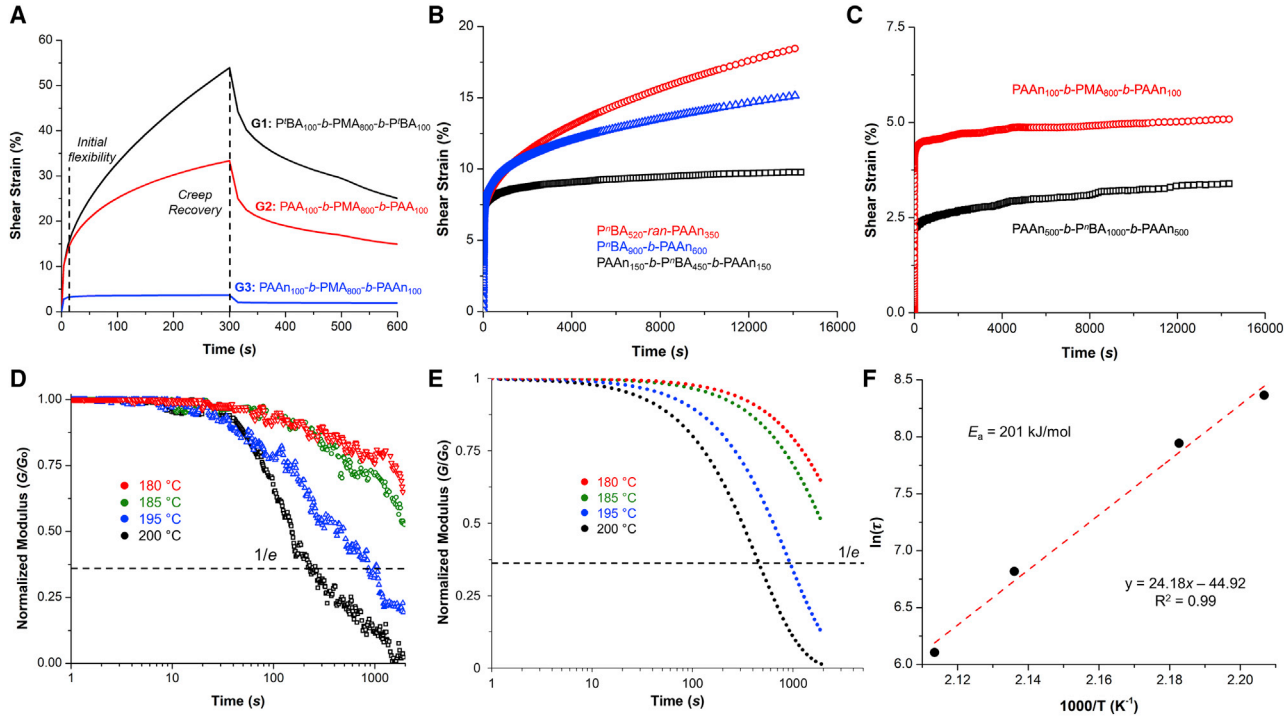

Figure 7. Rheology of G3 CANs

(A) Creep experiments (5 kPa, 100°C for G1 and G2 BCPs, 150°C for G3 network BCP).

(B) Creep comparison of G3 3:2 P^{n}BA/P^{t}BA random, di-BCP, and tri-BCP architectures (4 h, 200°C, 5 kPa).

(C) Additional G3 tri-BCP creep resistance experiments (4 h, 200°C, 5 kPa).

(D) Normalized-modulus stress-relaxation curves for P^{n}BA$_{520}$-*ran*-PAAn$_{350}$ (1-s rise time, 0.3% shear strain).

(E) Fitted stress-relaxation curves of P^{n}BA$_{520}$-*ran*-PAAn$_{350}$ used for extrapolating/deriving the characteristic relaxation values τ at 1/*e* normalized modulus.

(F) Arrhenius relationship plot for the E_a of the acid-anhydride exchange mechanism.

experiment compared with each of the tri-BCPs, including a noticeably larger creep deformation rate of 2.5 × 10^{-4}% strain per second (Figures 7B and 7C).

To directly isolate our unique ABA network as the key component responsible for creep suppression, we prepared another compositionally equivalent PMA-containing AB di-BCP (2:8, P^{t}BA$_{200}$-*b*-PMA$_{800}$, M_n = 3.86 × 10^5 g mol^{-1}, $Đ$ = 1.14; Figures S9, S15, S22, and S31) that exhibits strong self-assembly at the G2 and G3 stages to HPC nanostructures with *d*-spacing of 47–52 nm (Figure 8A). In a creep comparison between G3 di-BCP PAAn$_{200}$-*b*-PMA$_{800}$ and the tri-BCP analog (PAAn$_{100}$-*b*-PMA$_{800}$-*b*-PAAn$_{100}$), the G3 di-BCP exhibited higher creep (1.1% versus 0.6% shear strain) and creep deformation rates (8.0 × 10^5% versus 3.2 × 10^5% strain per second) (Figure 8B), which is consistent with the P^{n}BA-based BCPs creep results and our creep suppression by inter-domain exchange restriction hypothesis.

To further probe the acid-anhydride exchange mechanism, high-temperature frequency sweeps were performed on each G3 CAN at 170°C, 180°C, 190°C, and 200°C (0.1–10 Hz, 0.3% strain in compliance with linear viscoelasticity probed by initial strain sweeps; Figure S53). All G3 tri-BCPs behaved like characteristic thermosets with a constant storage modulus ($\Delta G' \approx 0$) at low frequencies and increased G' at higher frequencies, whereas the RCP exhibited an initial increase in modulus at low frequency that was exaggerated with increasing temperature (Figure S54). Although the G3 materials establish a near-consistent G' with increasing frequency,

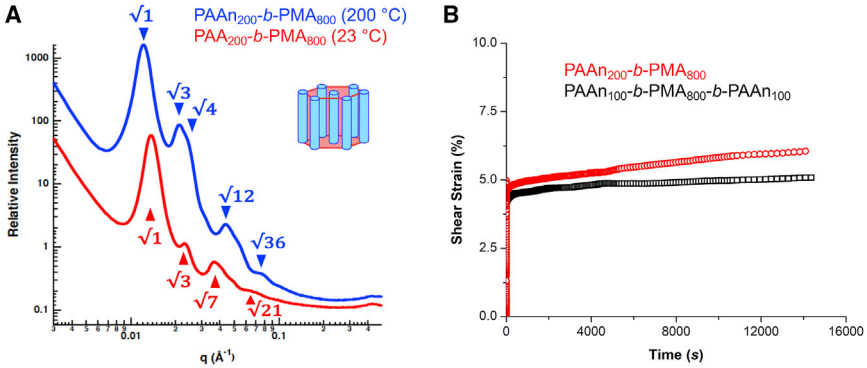

Figure 8. HPC G3 di- and tri-BCP comparison

(A) SAXS profiles of PMA-containing di-BCP films in G2 PAA (red, measured at 23°C) and G3 crosslinked PAAn (blue, measured at 200°C) HPCs.

(B) Creep comparison of G3 HPC 2:8 PMA/PAAn di-BCP and tri-BCP architectures (4 h, 200°C, 5 kPa).

indicative of constant crosslinking density under an associative exchange mechanism (Figure 1C), the slight drop in G' with increasing temperature also supports paralleling dissociative exchange via intra-molecular anhydride formation (Figure 1D), which would ultimately decrease G3 CAN crosslinking density (Figure S54).[46]

Last, we subjected the G3 BCP $PAAn_{150}$-*b*-P^nBA_{450}-*b*-$PAAn_{150}$ and RCP P^nBA_{520}-*ran*-$PAAn_{350}$ analogs to a series of stress-relaxation experiments to derive the activation energy (E_a) for the transition to a flow topology by the exchange mechanism. Again, in accordance with the lack of compression input available during rheological experiments and, thus, no reconfigurability, we did not observe a trend of reduced modulus for the tri-BCP within the experimental time (Figure S58). On the other hand, the compositional analog RCP without compression requirements exhibited characteristic relaxation of induced stress at longer timescales (t > 10–100 s) for temperatures of 180°C, 185°C, 195°C, and 200°C (Figure 7D). The normalized modulus for each temperature was fitted to an exponential decay curve, and the value τ (the time when $G'/G'_0 = 1/e$) was extrapolated under the appropriate assumption (all R^2 > 0.9) of a single Maxwell element (Figures 7D, 7E, and S56).[72] The obtained Arrhenius plot highlights a linear relationship where the slope of the linear-fit was used to calculate a high E_a of 201 kJ/mol (48.0 kcal/mol; Figures 7F and S57).

DISCUSSION

Here we developed not only a novel class of reprocessable thermosets based on nanostructured, dynamically crosslinked, all-acrylic tri-BCP TPEs but also a new thermomechanical activation mechanism responsible for the observed reprocessability and orthogonal working/reprocessing conditions. Such materials hold potential to provide a more sustainable alternative to non-recyclable or non-reprocessable crosslinked materials. Although here we focus on a few particular PAA-containing copolymers, we emphasize that virtually any PAA-containing polymer could be converted into similar CANs simply through heat-induced condensation. More importantly, through this self-preparation method, we introduce a CAN system that is independent of the external privileged crosslinkers, exchange agents, and catalysts typically necessary for dynamic bond exchange in reprocessable thermosets.

From a perspective of advanced polymer synthesis methods, our CSC-LPP synthesis of these ABA tri-BCPs is noteworthy in its own right because it is currently the only way to

Please cite this article in press as: Clarke et al., Thermomechanical activation achieving orthogonal working/healing conditions of nanostructured tri-block copolymer thermosets, Cell Reports Physical Science (2021), https://doi.org/10.1016/j.xcrp.2021.100483

generate such a high-MW polymer with such high precision, control, and timely manner at ambient temperature. The unique two-step propagation mechanism of LPP that involves bimolecular conjugate addition of a Lewis acid-stabilized enolate chain end to a Lewis acid-activated monomer provides compounded thermodynamic K_{eq} and kinetic k_p differentiation, allowing precise sequence control over polymerization of one-pot mixtures of comonomers.[60] Well-defined, all-acrylic tri-BCPs are challenging to synthesize even at low temperatures and at a small scale because of the uncontrollable reactivity, competing termination by facile acid-catalyzed de-*tert*-butylation of ^{t}BA, and predisposition to the Claisen-type termination of these monomers.[73,74] The CSC-LPP method facilitates synthesis of these well-defined tri-BCPs at ambient temperature and relatively large scales (35–70 g product) in a one-pot fashion in less than 5 min.

From a mechanistic point of view, our proposed acid/anhydride inter/intra-chain associative/dissociative dynamic exchange, under conditions by which we reprocess polymers, was supported by several lines of evidence, including the results obtained from the small-molecule model reactions and rheological frequency sweep experiments. Similarly, by rheological testing, we further probed the exchange mechanism by stress-relaxation on an analog RCP to access the standard CAN-type behavior. From these experiments, we were able to derive a rather high (composite) E_a for the acid/anhydride exchange of 201 kJ/mol, which can be attributed to the low nucleophilic character of carboxylic acids.

From a materials performance and reprocessability perspective, crosslinked G3 BCPs exhibit impressive mechanical performance with high modulus, toughness, and creep resistance as well as repeated reprocessability while maintaining mechanical integrity. The HPC assembly of the materials is credited for modulus and strength increases in going from G2 to the G3 phase, and contributions from the soft acrylic comonomers help give the materials flexibility to avoid the brittleness of many high-modulus materials. Our final point is the effect of BCP self-assembly and the networking effect of the ABA tri-BCP architecture. Crucial to this point is comparison of the RCP and the AB di-BCPs with the ABA tri-BCP compositional analogs. In the case of the RCP, any associative exchange might be productive in the mending or permanent reshaping of the overall structure because there is no domain spacing to compartmentalize exchange points. Similarly, although exchange points may be compartmentalized in the di-BCP, there is no inter-linked network to restrict productive reprocessing. In stark contrast, the tri-BCP has exchange points that are compartmentalized and, thus, not in contact with exchange points in other domains. This contrast can be observed in Figure 7B, where the RCP showed an ~10× increase and the di-BCP showed an ~5× increase in creep over a 4-h shear stress period. This hypothesis is further supported by direct comparison of G3 di- and tri-BCPs in Figure 8B, where the di-BCP exhibited an ~2× increase in creep deformation despite having the similarly self-assembled HPC nanostructure. When we consider time-dependent deformation of a domain-separated material, we hypothesize that exchange events occurring within a domain contribute negligibly to the overall creep. Therefore, mechanical force is required to put exchanging domains in contact with each other. This inter-domain exchange requirement provides a means to minimize creep during operating conditions while reserving the option to activate creep with collaborative thermomechanical reprocessing conditions.

EXPERIMENTAL PROCEDURES

Resource availability

Lead contact

Further information and requests for resources and reagents should be directed to and will be fulfilled by the lead contact, Eugene Y.-X. Chen (eugene.chen@colostate.edu).

Materials availability

This study did not generate new unique materials.

Data and code availability

All data needed to evaluate the conclusions in this paper are present in the paper and/or the Supplemental information.

SUPPLEMENTAL INFORMATION

Supplemental information can be found online at https://doi.org/10.1016/j.xcrp.2021.100483.

ACKNOWLEDGMENTS

We gratefully acknowledge financial support from the US Army Research Office (W911NF1810435) for R.W.C.'s work and the U.S. National Science Foundation (NSF-1904962) for M.L.M.'s work. Synchrotron SAXS data were collected at Sector 12 in the X-Ray Science Division of the Advanced Photon Source, a U.S. Department of Energy (DOE) Office of Science User Facility operated for the DOE Office of Science by Argonne National Laboratory under contract DE-AC02-06CH11357. We thank A. Klug and A. Winter in the Bailey group for assistance with SAXS analysis and Dr. B. Boyle in the Miyake group for assistance with mechanical and rheological analyses.

AUTHOR CONTRIBUTIONS

R.W.C., M.L.M., and E.Y.-X.C. conceived the idea and designed the experiments. R.W.C. and M.L.M. carried out the experiments, and B.S.N. collected SAXS data and processed data. R.W.C., M.L.M., and E.Y.-X.C. co-wrote the manuscript, and all authors participated in data analyses and discussions and read and edited the manuscript. E.Y.-X.C. directed the project.

DECLARATION OF INTERESTS

The authors declare no competing interests.

Received: April 4, 2021
Revised: May 14, 2021
Accepted: June 7, 2021
Published: July 1, 2021

REFERENCES

1. Hong, M., and Chen, E.Y.-X. (2019). Future Directions for Sustainable Polymers. Trends Chem. *1*, 148–151.
2. Zhang, X., Fevre, M., Jones, G.O., and Waymouth, R.M. (2018). Catalysis as an Enabling Science for Sustainable Polymers. Chem. Rev. *118*, 839–885.
3. Schneiderman, D.K., and Hillmyer, M.A. (2017). 50th Anniversary Perspective: There Is a Great Future in Sustainable Polymers. Macromolecules *50*, 3733–3749.
4. Hong, M., and Chen, E.Y.-X. (2017). Chemically Recyclable Polymers: A Circular Economy Approach to Sustainability. Green Chem. *19*, 3692–3706.
5. Tang, X., and Chen, E.Y.-X. (2019). Towards Infinitely Recyclable Plastics Derived from Renewable Cyclic Esters. Chem *5*, 284–312.
6. Geyer, R., Jambeck, J.R., and Law, K.L. (2017). Production, use, and fate of all plastics ever made. Sci. Adv. *3*, e1700782.
7. Garcia, J.M., and Robertson, M.L. (2017). The future of plastics recycling. Science *358*, 870–872.
8. Lu, X.-B., Liu, Y., and Zhou, H. (2018). Learning nature: recyclable monomers and polymers. Chemistry *24*, 11255–11266.
9. Zhu, Y., Romain, C., and Williams, C.K. (2016). Sustainable polymers from renewable resources. Nature *540*, 354–362.
10. Coates, G.W., and Getzler, Y.D.Y.L. (2020). Chemical recycling to monomer for an ideal, circular polymer economy. Nat. Rev. Mater. *5*, 501–516.
11. Rahimi, A., and García, J.M. (2017). Chemical recycling of waste plastics for new materials production. Nat. Rev. Chem. *1*, e0046.
12. Zheng, N., Xu, Y., Zhao, Q., and Xie, T. (2021). Dynamic Covalent Polymer Networks: A Molecular Platform for Designing Functions beyond Chemical Recycling and Self-Healing. Chem. Rev. *121*, 1716–1745.
13. Zhu, J.-B., Watson, E.M., Tang, J., and Chen, E.Y.-X. (2018). A synthetic polymer system with repeatable chemical recyclability. Science *360*, 398–403.

14. Hong, M., and Chen, E.Y.-X. (2016). Completely recyclable biopolymers with linear and cyclic topologies via ring-opening polymerization of γ-butyrolactone. Nat. Chem. *8*, 42–49.

15. Shi, C., Li, Z.-C., Caporaso, L., Cavallo, L., Falivene, L., and Chen, E.Y.-X. (2021). Hybrid Monomer Design for Unifying Conflicting Polymerizability, Recyclability, Performance Properties. Chem *7*, 680–685.

16. Delle Chiaie, K.R., McMahon, F.R., Williams, E.J., Price, M.J., and Dove, A.P. (2020). Dual-Catalytic Depolymerization of Polyethylene Terephthalate (PET). Polym. Chem. *11*, 1450–1453.

17. Fukushima, K., Lecuyer, J.M., Wei, D.S., Horn, H.W., Jones, G.O., Al-Megren, H.A., Alabdulrahman, A.M., Alsewailem, F.D., McNeil, M.A., Rice, J.E., and Hedrick, J.L. (2013). Advanced Chemical Recycling of Poly(Ethylene Terephthalate) through Organocatalytic Aminolysis. Polym. Chem. *4*, 1610–1616.

18. Rorrer, N.A., Nicholson, S., Carpenter, A., Biddy, M.J., Grundl, N.J., and Beckham, G.T. (2019). Combining Reclaimed PET with Biol.-based Monomers Enables Plastics Upcycling. Joule *3*, 1006–1027.

19. Easterling, C.P., Kubo, T., Orr, Z.M., Fanucci, G.E., and Sumerlin, B.S. (2017). Synthetic upcycling of polyacrylates through organocatalyzed post-polymerization modification. Chem. Sci. (Camb.) *8*, 7705–7709.

20. Lepage, M.L., Simhadri, C., Liu, C., Takaffoli, M., Bi, L., Crawford, B., Milani, A.S., and Wulff, J.E. (2019). A broadly applicable cross-linker for aliphatic polymers containing C-H bonds. Science *366*, 875–878.

21. Lessard, J.J., Scheutz, G.M., Sung, S.H., Lantz, K.A., Epps, T.H., 3rd, and Sumerlin, B.S. (2020). Block Copolymer Vitrimers. J. Am. Chem. Soc. *142*, 283–289.

22. Lessard, J.J., Garcia, L.F., Easterling, C.P., Sims, M.B., Bentz, K.C., Arencibia, S., Savin, D.A., and Sumerlin, B.S. (2019). Catalyst-Free Vitrimers from Vinyl Polymers. Macromolecules *52*, 2105–2111.

23. Tretbar, C.A., Neal, J.A., and Guan, Z. (2019). Direct Silyl Ether Metathesis for Vitrimers with Exceptional Thermal Stability. J. Am. Chem. Soc. *141*, 16595–16599.

24. Röttger, M., Domenech, T., van der Weegen, R., Breuillac, A., Nicolaÿ, R., and Leibler, L. (2017). High-performance vitrimers from commodity thermoplastics through dioxaborolane metathesis. Science *356*, 62–65.

25. Denissen, W., Winne, J.M., and Du Prez, F.E. (2016). Vitrimers: permanent organic networks with glass-like fluidity. Chem. Sci. (Camb.) *7*, 30–38.

26. García, J.M., Jones, G.O., Virwani, K., McCloskey, B.D., Boday, D.J., ter Huurne, G.M., Horn, H.W., Coady, D.J., Bintaleb, A.M., Alabdulrahman, A.M.S., et al. (2014). Recyclable, strong thermosets and organogels via paraformaldehyde condensation with diamines. Science *344*, 732–735.

27. Montarnal, D., Capelot, M., Tournilhac, F., and Leibler, L. (2011). Silica-like malleable materials from permanent organic networks. Science *334*, 965–968.

28. Hayashi, M., and Chen, L. (2020). Functionalization of triblock copolymer elastomers by cross-linking the end blocks via trans-*N*-alkylation-based exchangeable bonds. Polym. Chem. *11*, 1713–1719.

29. Kloxin, C.J., Scott, T.F., Adzima, B.J., and Bowman, C.N. (2010). Covalent Adaptable Networks (CANs): A Unique Paradigm in Crosslinked Polymers. Macromolecules *43*, 2643–2653.

30. Bowman, C.N., and Kloxin, C.J. (2012). Covalent adaptable networks: reversible bond structures incorporated in polymer networks. Angew. Chem. Int. Ed. Engl. *51*, 4272–4274.

31. Jin, Y., Yu, C., Denman, R.J., and Zhang, W. (2013). Recent advances in dynamic covalent chemistry. Chem. Soc. Rev. *42*, 6634–6654.

32. Taynton, P., Yu, K., Shoemaker, R.K., Jin, Y., Qi, H.J., and Zhang, W. (2014). Heat- or water-driven malleability in a highly recyclable covalent network polymer. Adv. Mater. *26*, 3938–3942.

33. Cromwell, O.R., Chung, J., and Guan, Z. (2015). Malleable and Self-Healing Covalent Polymer Networks through Tunable Dynamic Boronic Ester Bonds. J. Am. Chem. Soc. *137*, 6492–6495.

34. Jin, K., Li, L., and Torkelson, J.M. (2016). Recyclable Crosslinked Polymer Networks via One-Step Controlled Radical Polymerization. Adv. Mater. *28*, 6746–6750.

35. Zou, W., Dong, J., Luo, Y., Zhao, Q., and Xie, T. (2017). Dynamic Covalent Polymer Networks: from Old Chemistry to Modern Day Innovations. Adv. Mater. *29*, e1606100.

36. Ogden, W.A., and Guan, Z. (2018). Recyclable, Strong, and Highly Malleable Thermosets Based on Boroxine Networks. J. Am. Chem. Soc. *140*, 6217–6220.

37. Zou, Z., Zhu, C., Li, Y., Lei, X., Zhang, W., and Xiao, J. (2018). Rehealable, fully recyclable, and malleable electronic skin enabled by dynamic covalent thermoset nanocomposite. Sci. Adv. *4*, eaaq0508.

38. Fortman, D.J., Brutman, J.P., De Hoe, G.X., Snyder, R.L., Dichtel, W.R., and Hillmyer, M.A. (2018). Approaches to Sustainable and Continually Recyclable Cross-Linked Polymers. ACS Sustain. Chem.& Eng. *6*, 11145–11159.

39. Scheutz, G.M., Lessard, J.J., Sims, M.B., and Sumerlin, B.S. (2019). Adaptable Crosslinks in Polymeric Materials: Resolving the Intersection of Thermoplastics and Thermosets. J. Am. Chem. Soc. *141*, 16181–16196.

40. Christensen, P.R., Scheuermann, A.M., Loeffler, K.E., and Helms, B.A. (2019). Closed-loop recycling of plastics enabled by dynamic covalent diketoenamine bonds. Nat. Chem. *11*, 442–448.

41. Podgórski, M., Spurgin, N., Mavila, S., and Bowman, C.N. (2020). Mixed mechanisms of bond exchange in covalent adaptable networks: monitoring the contribution of reversible exchange and reversible addition in thiol–succinic anhydride dynamic networks. Polym. Chem. *11*, 5365–5376.

42. Kloxin, C.J., and Bowman, C.N. (2013). Covalent adaptable networks: smart, reconfigurable and responsive network systems. Chem. Soc. Rev. *42*, 7161–7173.

43. Chakma, P., and Konkolewicz, D. (2019). Dynamic Covalent Bonds in Polymeric Materials. Angew. Chem. Int. Ed. Engl. *58*, 9682–9695.

44. Roy, N., Bruchmann, B., and Lehn, J.-M. (2015). DYNAMERS: dynamic polymers as self-healing materials. Chem. Soc. Rev. *44*, 3786–3807.

45. Wojtecki, R.J., Meador, M.A., and Rowan, S.J. (2011). Using the dynamic bond to access macroscopically responsive structurally dynamic polymers. Nat. Mater. *10*, 14–27.

46. Jourdain, A., Asbai, R., Anaya, O., Chehimi, M.M., Drockenmuller, E., and Montarnal, D. (2020). Rheological Properties of Covalent Adaptable Networks with 1,2,3-Triazolium Cross-Links: The Missing Link between Vitrimers and Dissociative Networks. Macromolecules *53*, 1884–1900.

47. Podgórski, M., Fairbanks, B.D., Kirkpatrick, B.E., McBride, M., Martinez, A., Dobson, A., Bongiardina, N.J., and Bowman, C.N. (2020). Toward Stimuli-Responsive Dynamic Thermosets through Continuous Development and Improvements in Covalent Adaptable Networks (CANs). Adv. Mater. *32*, e1906876.

48. Chen, Y., Kushner, A.M., Williams, G.A., and Guan, Z. (2012). Multiphase design of autonomic self-healing thermoplastic elastomers. Nat. Chem. *4*, 467–472.

49. Jin, Y., Lei, Z., Taynton, P., Huang, S., and Zhang, W. (2019). Malleable and Recyclable Thermosets: The Next Generation of Plastics. Matter *1*, 1456–1493.

50. Fortman, D.J., Brutman, J.P., Cramer, C.J., Hillmyer, M.A., and Dichtel, W.R. (2015). Mechanically activated, catalyst-free polyhydroxyurethane vitrimers. J. Am. Chem. Soc. *137*, 14019–14022.

51. Feng, H., Lu, X., Wang, W., Kang, N.-G., and Mays, J.W. (2017). Block Copolymers: Synthesis, Self-Assembly, and Applications. Polymers (Basel) *9*, e494.

52. Uhrig, D., and Mays, J.W. (2002). Synthesis of Combs, Centipedes, and Barbwires: Poly(Isoprene-Graft-Styrene) Regular Multigraft Copolymers with Trifunctional, Tetrafunctional, and Hexafunctional Branch Points. Macromolecules *35*, 7182–7190.

53. Bates, C.M., and Bates, F.S. (2017). 50th Anniversary Perspective: Block Polymers—Pure Potential. Macromolecules *50*, 3–22.

54. Mai, Y., and Eisenberg, A. (2012). Self-assembly of block copolymers. Chem. Soc. Rev. *41*, 5969–5985.

55. Matsen, M.W., and Bates, F.S. (1996). Origins of Complex Self-Assembly in Block Copolymers. Macromolecules *29*, 7641–7644.

56. Ishibashi, J.S.A., Pierce, I.C., Chang, A.B., Zografos, A., El-Zaatari, B.M., Fang, Y., Weigand, S.J., Bates, F.S., and Kalow, J.A. (2021). Mechanical and Structural Consequences of Associative Dynamic Cross-

linking in Acrylic Diblock Copolymers. Macromolecules *54*, 3972–3986.

57. Yang, C.Q. (1993). Infrared Spectroscopy Studies of the Cyclic Anhydride as the Intermediate for the Ester Crosslinking of Cotton Cellulose by Polycarboxylic Acids. I. Identification of the Cyclic Anhydride Intermediate. J. Polym. Sci. A Polym. Chem. *31*, 1187–1193.

58. Lin, S.-Y., Cheng, W.-T., Wei, Y.-S., and Lin, H.-L. (2011). DSC-FTIR Microspectroscopy Used to Investigate the Heat-Induced Intramolecular Cyclic Anhydride Formation between Eudragit E and PVA Copolymer. Polym. J. *43*, 577–580.

59. Filippov, A.D., van Hees, I.A., Fokkink, R., Voets, I.K., and Kamperman, M. (2018). Rapid and Quantitative De-*tert*-butylation for Poly(acrylic acid) Block Copolymers and Influence on Relaxation of Thermoassociated Transient Networks. Macromolecules *51*, 8316–8323.

60. Qiao, Z., Qiu, T., Liu, W., Guo, L., and Li, X. (2016). Novel tri-block copolymers of poly(acrylic acid)- b-poly(2,2,3,3,4,4,4-hexafluorobutyl acrylate)-*b*-poly(acrylic acid) prepared via two-step RAFT emulsion polymerization. Polym. Chem. *7*, 3993–3997.

61. Li, H.G., Yang, P.P., Gao, S.Z., and Zhu, Y.Q. (2012). Synthesis and micellar behavior of poly(acrylic acid-b-styrene) block copolymers. Colloid Polym. Sci. *290*, 1825–1831.

62. Schaefgen, J.R., and Sarasohn, I.M. (1962). Observations on the thermolytic decomposition of poly(tert-butyl acrylate). J. Polym. Sci. *58*, 1049–1061.

63. Grant, D.H., and Grassie, N. (1960). The thermal decomposition of poly(*t*-butyl methacrylate). Polymer (Guildf.) *1*, 445–455.

64. McGraw, M.L., Clarke, R.W., and Chen, E.Y.-X. (2020). Compounded Sequence Control in Polymerization of One-Pot Mixtures of Highly Reactive Acrylates by Differentiating Lewis Pairs. J. Am. Chem. Soc. *142*, 5969–5973.

65. Lawton, M.I., Tillman, K.R., Mohammed, H.S., Kuang, W., Shipp, D.A., and Mather, P.T. (2016). Anhydride-Based Reconfigurable Shape Memory Elastomers. ACS Macro Lett. *5*, 203–207.

66. Colombani, O., Ruppel, M., Schubert, F., Zettl, H., Pergushov, D.V., and Müller, A.H.E. (2007). Synthesis of Poly(*n*-butyl acrylate)-*block*-poly(acrylic acid) Diblock Copolymers by ATRP and Their Micellization in Water. Macromolecules *40*, 4338–4350.

67. Vidal, F., Watson, E.M., and Chen, E.Y.-X. (2019). All-Methacrylic Stereoregular Triblock Co-Polymer Thermoplastic Elastomers Toughened by Supramolecular Stereocomplexation. Macromolecules *52*, 7313–7323.

68. Watts, A., Kurokawa, N., and Hillmyer, M.A. (2017). Strong, Resilient, and Sustainable Aliphatic Polyester Thermoplastic Elastomers. Biomacromolecules *18*, 1845–1854.

69. Pitet, L.M., Chamberlain, B.M., Hauser, A.W., and Hillmyer, M.A. (2019). Dispersity and Architecture Driven Self-Assembly and Confined Crystallization of Symmetric Branched Block Copolymers. Polym. Chem. *10*, 5385–5395.

70. Shim, J., Bates, F.S., and Lodge, T.P. (2019). Superlattice by charged block copolymer self-assembly. Nat. Commun. *10*, 2108.

71. Kim, K., Schulze, M.W., Arora, A., Lewis, R.M., 3rd, Hillmyer, M.A., Dorfman, K.D., and Bates, F.S. (2017). Thermal processing of diblock copolymer melts mimics metallurgy. Science *356*, 520–523.

72. Goodwin, J.W., and Hughes, R.W. (2008). Rheology for Chemists: An Introduction (Royal Society of Chemistry).

73. Jia, Y.-B., Wang, Y.-B., Ren, W.-M., Xu, T., Wang, J., and Lu, X.-B. (2014). Mechanistic Aspects of Initiation and Deactivation in N-Heterocyclic Olefin Mediated Polymerization of Acrylates with Alane as Activator. Macromolecules *47*, 1966–1972.

74. He, J., Zhang, Y., Falivene, L., Caporaso, L., Cavallo, L., and Chen, E.Y.-X. (2014). Chain Propagation and Termination Mechanisms for Polymerization of Conjugated Polar Alkenes by [Al]-Based Frustrated Lewis Pairs. Macromolecules *47*, 7765–7774.